Sensors & Actuators: B. Chemical 355 (2022) 131298

Contents lists available at ScienceDirect

Sensors and Actuators: B. Chemical

journal homepage: www.elsevier.com/locate/snb

Non-enzymatic electrochemical detection of H_2O_2 by assembly of CuO nanoparticles and black phosphorus nanosheets for early diagnosis of periodontitis

Kun Wang [a], Yue Sun [a], Wenzhou Xu [a], Wei Zhang [a], Fanrou Zhang [a], Yu Qi [b], Yuhong Zhang [b], Qingqing Zhou [b], Biao Dong [b], Chunyan Li [a], Lin Wang [a,*], Lin Xu [b,*]

[a] Department of Oral Implantology, Jilin Provincial Key Laboratory of Sciences and Technology for Stomatology Nanoengineering, Hospital of Stomatology, Jilin University, Changchun 130021, China
[b] State Key Laboratory on Integrated Optoelectronics, Collage of Electronic Science and Engineering, Jilin University, Changchun 130021, China

ARTICLE INFO

Keywords:
Biosensor
Periodontitis
Transition metal oxides
Two-dimensional materials
Hydrogen peroxide
Live cells

ABSTRACT

Periodontitis, as one of the most universal chronic inflammatory diseases worldwide, has raised numerous attentions since its tremendous destructive force against alveolar bone and soft tissue, ultimately leading to the tooth loss. Hydrogen peroxide (H_2O_2) is a major byproduct during the pathogenesis of periodontitis, which hints that direct and in-situ detection of H_2O_2 provides an effective way for early diagnosis of periodontitis. Herein, a non-enzymatic and highly electrocatalytic H_2O_2 biosensor was proposed by using a novel electrode composed of copper oxide nanoparticles (CuO NPs), black phosphorus nanosheets (BP NSs) and chitosan. Owing to the remarkable electrochemical redox capability of CuO NPs and marvelous conductivity of BP NSs, such heterostructure attained enhanced surface adsorption and efficient electron transfer, contributing to ultrasensitive determination of H_2O_2 in a real-time manner. The synergistic effects of CuO and BP demonstrated supreme electrocatalytic ability with a low practical detection limit (30 nM), excellent sensitivity (138.00 μA mM^{-1} cm^{-2}), extraordinary selectivity, splendid reusability and long-term stability. In terms of biofluid level, this biosensor achieved feasible detection of H_2O_2 in saliva and gingival crevicular fluid samples and effectively differentiated patients of periodontitis from healthy people, which lay solid foundation for diagnosis of periodontitis. Referring to cellular scale, such device was successfully implemented to detect H_2O_2 released from macrophages and gingival fibroblasts, presenting favorable biosensing capability in living cells. Looking forward, this design of CuO/BP sensor could be extended to broader applications in monitoring physiological and dynamic in-clinic pathological processes in other inflammatory diseases.

1. Introduction

Periodontitis, as the sixth prevalent chronic inflammatory disease, is regarded as one of the most important global oral health burdens since it was found in approximate 50% of the population and also closely related with numerous systematic diseases including diabetes, cardiovascular disease, Alzheimer's disease, *etc* [1]. Once periodontitis initiates, the damage of periodontal tissue is almost inevitable and irreversible. If left untreated, periodontitis would ultimately lead to the tooth loss. Currently, periodontitis is diagnosed almost entirely on the basis of its clinical manifestations such as indexes of gingival inflammation, probing depth for periodontal attachment or radiographic examinations for alveolar bone loss. However, the early stages of periodontitis are still difficult to identify and quantify due to the lack of an effectively linear diagnostic tool and inconspicuous clinical indications.

For last decades, ongoing efforts have been made on exploring novel biomarkers in saliva for diagnosis of periodontitis [2]. The alteration of cytokine levels like interleukin-1β (IL-1β) and tumor necrosis factor-α (TNF-α) in saliva are verified to be associated with the inflammatory response of periodontal tissue [3]. Whereas, the detection of such cytokines is accompanied with the utilization of antibody which is high-cost, easily inactive, and complicated in immobilized procedure. Inspiringly, extensive evidences confirmed that reactive oxygen species (ROS) such as hydrogen peroxide (H_2O_2) acted a significant role in the

* Corresponding authors.
E-mail addresses: wanglin1982@jlu.edu.cn (L. Wang), linxu@jlu.edu.cn (L. Xu).

https://doi.org/10.1016/j.snb.2021.131298
Received 6 September 2021; Received in revised form 14 December 2021; Accepted 18 December 2021
Available online 22 December 2021

pathogenesis of periodontitis [4]. Furthermore, a rising level of H_2O_2 was spotted in gingival crevicular fluid (GCF) and saliva for individuals with periodontitis, exactly indicating underlying inflammation response [5]. Therefore, it is urgently desirable to develop a sensing system for determining H_2O_2 level in GCF and saliva for early diagnosis of periodontitis, and meanwhile achieving rapid, accurate, and non-invasive sensing platform to be beneficial to the timely intervention and guidance for therapeutics.

Until now, tremendous progresses have been made to monitor H_2O_2 concentration by various approaches such as chemiluminescence, fluorometry, colorimetry, *etc* [6]. However, these methods still suffer from expensive charge, complex instrumentations, long operating time as well as inaccessibility for the general public without systematic expertise. Recently, electrochemical detection of H_2O_2 has raised much interest for its unparalleled sensitivity and low detection limit. Particularly, non-enzymatic sensors take prevalence owing to the simple fabrication procedure, favorable repeatability, excellent electrocatalytic activity, and superior adaptation for monitoring H_2O_2 [7]. In enzyme-free electrochemical systems, transition metal oxides (TMOs) have been widely employed in biosensors on account of supreme electrochemical stability and environmental compatibility [8]. Thereinto, copper oxide (CuO) nanostructures as a p-type semiconductor with a narrow band gap of 1.2 eV, have been deeply exploited and perform prominent efficiency due to its remarkable electrochemical redox capability as well as large catalytic active areas. Nevertheless, its weak combination, inferior cyclic stability and poor electron conductivity ($\approx 10^{-3}$ S m^{-1}) have strongly limited the physiological application for electrochemical detection of H_2O_2 [9], The effective strategy to enhance the electrochemical performance of CuO sensors can be summarized as the following approaches: morphology modulation in size and specific surface area, defect engineering in electronic structure and inherent capability, and heterostructure construction in building hierarchical materials pairs, *etc* [10,11]. Among these methods, heterostructure construction is an effective and simple method for enhancing the catalytic capabilities of the electrocatalyst by constructing novel hierarchical components [12]. Compared with bare CuO, heterostructure design attains marvelous electrochemical sensing competence, such as enhanced recognizing and differentiating capacity for higher sensitivity and better selectivity [13], which is attributed to multiplication of electron absorption capability and interfacial charge transport from each component.

Recently, two-dimensional (2D) materials attract more and more interest since the successful isolation of graphene from graphite in 2004 on account of completely unexpected and extraordinary properties [14]. Specifically, with almost single atomic thickness layer-dependent bandgap, moderate carrier mobility, large surface-area-to-volume, 2D materials are definitely ideal candidate for use in biosensing, bioimaging, photothermal therapy, photodynamic therapy, and drug delivery [15]. Black phosphorus (BP), a particularly appealing 2D nanomaterial in the post-graphene era, is the most stable allotrope of phosphorus elements [16]. As 2D material, BP is advantageous for large specific surface area, high electron mobility (10^4 cm^2 V^{-1} s^{-1}), short ion diffusion channels, and robust mechanical flexibility. Compared to other 2D materials like graphene and transition-metal dichalcogenides, BP shows outstanding biocompatibility and favorable biodegradability in the body, which makes it an optimum choice for various biological arrays and extensively applied in electrochemical sensors. Until now, Yan et al. have demonstrated a non-enzymatic H_2O_2 sensor based on few-layer BP for the first time to utilize BP degradation under ambient conditions [17]. Zhao et al. have proposed a simple, noncovalent modification strategy to synthesize poly-L-lysine-black phosphorus (pLL-BP) hybrid, which displays excellent catalytic activity toward the reduction of oxygen and hydrogen peroxide [18]. Zhao et al. have fabricated a copper–chitosan–black phosphorus nanocomposite (CuNPs-Chit-BP) for monitoring H_2O_2, which proposed a new strategy to explore novel BP-based non-enzymatic biosensing platforms [19]. All biosensors mentioned above obtain supreme electrochemical detecting performance with addition of BP owing to the inherent electronic and biological character especially the high carrier mobility and fabulous biocompatibility. However, the sensing performance of the combination of BP and TMOs (such as CuO, ZnO, *etc*) are not yet investigated especially as a biosensor to detect H_2O_2 in cellular level or in biofluids for early diagnosis of periodontitis.

Herein, we designed and fabricated an electrochemical biosensor with copper oxide nanoparticles (CuO NPs) anchoring onto black phosphorus nanosheets (BP NSs) for sensitive and selective detection of H_2O_2 with high affinity and recognition capabilities. Combining extraordinary surface absorption capability of CuO and excellent interfacial electron mobility of BP, such biosensor demonstrated brilliant sensitivity, reusability and stability. Furthermore, with superior selectivity, it allowed for precise recognition and diagnosis of early periodontitis using human gingival crevicular fluid (GCF) and saliva samples. Moreover, great potential has been explored for rapid and direct detection of secretion of H_2O_2 in a cellular level upon external stimulation. This work paves the way of accurate detection of H_2O_2 for early diagnosis and treatment in terms of diseases more than periodontitis.

2. Results and discussion

2.1. Characterization of CuO NPs/BP NSs samples

Fig. 1A depicted the schematic preparation process of CuO/BP nanocomposites and subsequent modification of the electrode. The morphology and surface characteristics of as-prepared samples were first illuminated by TEM images. Fig. 1B showed the uniform and spherical CuO NPs with the diameter in range of 10-50 nm, even after surface modified with CTAB. While, Fig. 1C confirmed the successful inheritance of the typical lamellar morphology of BP NSs. After mixing, the CuO NPs could uniformly disperse onto the few-layer BP NSs (Fig. 1D) due to the mutual electrostatic adsorption. The heterostructure of CuO/BP was also proved by SEM images (Fig. S1), in which CuO NPs were well and clearly anchoring on wrinkled BP NSs. In detail, the HRTEM images exhibited apparent lattice fringes with an interplanar spacing of 0.232 nm (Fig. 1E and G), which agreed well with the (111) plane of cubic CuO. In Fig. 1F and G, the lattice fringes of 0.26 nm were attributed to the (040) plane of BP, further confirmed the well combination of CuO NPs and BP NSs. In addition, the EDS mapping were employed to determine the element distribution and purity of the prepared CuO/BP hybrid. As shown in Fig. S1, the hybrid consisted of O, Cu and P elements, and all the elements were uniformly distributed throughout the whole sample. All above results indicated that the CuO NPs were homogeneously coated on the BP layers in the CuO/BP hybrid structure due to electrostatic adsorption. Moreover, such unique heterostructure contributed to enlargement of surface area and enhancement of electron-transfer processes, which accounted a lot for electrochemical detection of trace amount of H_2O_2.

Besides HRTEM, the crystal structure of the CuO/BP composite was elucidated by XRD spectra. As shown in Fig. 2**A**, two strong peaks centered at 35.5° and 38.6° were corresponding to the (002) and (111) planes of CuO (JCPDS#80-1917), respectively. Two typical diffraction peaks at 17.0° and 34.3° were well indexed to the (020) and (040) planes of BP (JCPDS#73-1358). Notably, the distinct peaks of BP were weaker in the XRD pattern of nanohybrid, which could be attributed to the reaction process accompanied with the oxidation of few-layer BP and formation of P_xO_y during the individual reaction [20]. These results confirmed the successful formation of composite structure of CuO/BP. The variation in the Raman spectra for CuO, BP, and final CuO/BP hybrids was plotted in Fig. 2**B**. Three typical Raman peaks in spectra of CuO were situated at 283, 328 and 628 cm^{-1}. While, the symbolization of bare BP was represented by three characteristic peaks centered at 363.7, 441.0, and 469.5 cm^{-1}, corresponding to A^1_g, B^2_g, and A^2_g

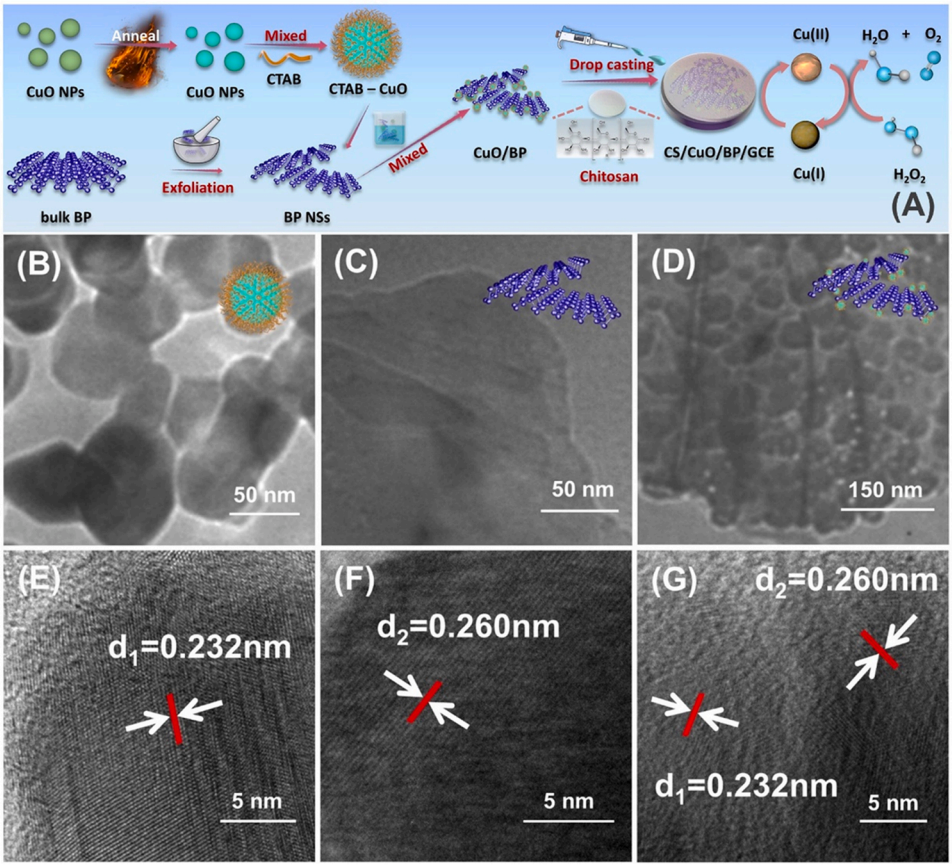

Fig. 1. (A) Formation of the CuO/BP nanocomposites: the annealed CuO NPs were modified by CTAB, and then anchored onto the exfoliated BP NSs by mixing in solution. The stepwise process for the modified electrode: the CuO/BP nanocomposites and CS were dropped onto the GCE sequentially. The electrooxidation mechanism on the prepared electrode: conversion from H_2O_2 to H_2O and O_2 is in accordance with valence change of Cu. Characterization of CuO/BP nanocomposites: (B-D) Typical TEM images and (E-G) corresponding HRTEM images of (B, E) CuO NPs, (C, F) BP NSs, and (D, G) CuO/BP nanocomposites.

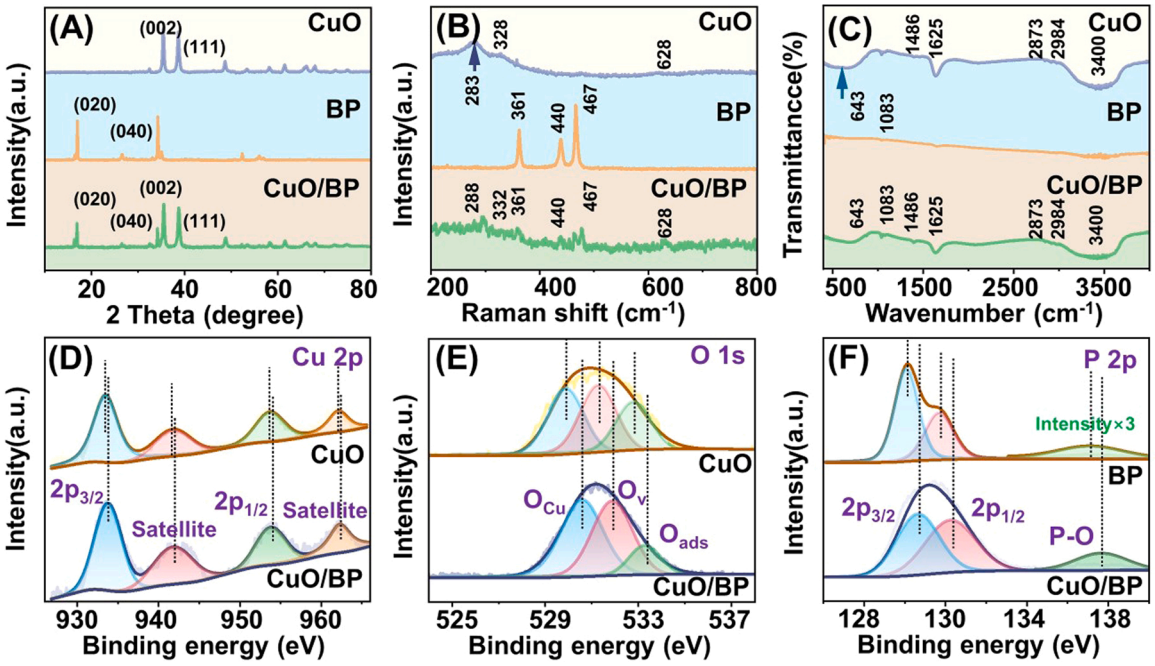

Fig. 2. Surface morphology analysis of CuO/BP nanocomposites: (A) XRD patterns, (B) Raman spectra, and (C) FTIR patterns of CuO, BP and CuO/BP; high-resolution XPS spectra of (D) Cu 2p, (E) O 1s and (F) P 2p.

vibrational modes, respectively. For the CuO/BP nanocomposites, the shift for distinct peaks compared with those of pure CuO and bare BP indicated an intimate interfacial interaction between different contents of the hybrid [21].

In addition, the vibrational modes of pure nanomaterials and nanohybrid were also explored by the FTIR spectra to serve as evidence of heterostructure formation. Fig. 2**C** depicted the FTIR spectra of CuO, BP and CuO/BP nanocomposites. For CuO NPs, the band lined at 643 cm^{-1}

can be attributed to the Cu(II)–O elastic vibration [22]. Furthermore, the O–H stretching band was situated at 1625 and 3400 cm^{-1}, which suggested the existence of hydroxyl ions due to the metal-OH layer [23]. In terms of CTAB, the tiny bands in the region of 1426 cm^{-1} were attributed to the deformation of -CH_2- and -CH_3 groups in the incorporated surfactants. Subsequently, the weak bands detected at 2984 and 2873 cm^{-1} were ascribed to C-CH_2 asymmetric stretching and N-CH_3 symmetric stretching vibrations of the solid and the surfactant, respectively [24]. As for BP NSs, the P-O absorption band was observed at 1083 cm^{-1}. All bands mentioned above were spotted in the spectra for CuO/BP nanocomposites, confirming the successful formation of such unique heterostructures. Furthermore, the Cu(II)–O elastic vibration was relatively weaker in the hybrid sample compared with bare CuO NPs, demonstrating interfacial interaction of the nanocomposites.

The surface element information (such as valance state and composition) of the CuO/BP composite were obtained through XPS analysis. The XPS survey spectrum in Fig. S2 demonstrated the presence of Cu, O, C, Br and P elements. The high-resolution Cu 2p spectrum of CuO and CuO/BP composite (Fig. 2**D**) showed two main peaks centered at 933.6 and 953.3 eV, along with two corresponding satellite peaks located at 941.7 and 961.4 eV. The two main peak were assigned to Cu $2p_{3/2}$ and Cu $2p_{1/2}$, respectively. Compared with pure CuO, there was a slight shift for Cu 2p peak towards higher binding energy in CuO/BP composite, indicating a modification of the electron density on CuO due to the interactive coupling between CuO and BP. The broad Cu $2p_{3/2}$ peak had been decomposed into two peaks related to Cu(I) and Cu(II) respectively [25]. The Cu(I) peak for CuO and CuO/BP were situated at 932.1 and 932.6 eV , the binding energy of Cu(II) peak was 934.3 eV for CuO and 934.7 eV for CuO/BP [26]. Moreover, the [Cu(I)/Cu(I)+Cu(II)] area ratios in the Cu $2p_{3/2}$ peak were calculated to be 36.0% and 40.5% for CuO and CuO/BP samples respectively. All mentioned above indicated the existence of Cu(I) and its increase in CuO/BP samples compared with bare CuO samples. This phenomenon may be assigned to the reason that excellent interfacial electron mobility of BP facilitates the whole redox process [27]. According to binding energy of O 1 s (Fig. 2**E**), the XPS spectra of CuO can be deconvoluted into three peaks: lattice oxygen (O_{Cu}), deficient oxygen (O_v), and adsorbed oxygen (O_{ads}) species, with corresponding peak intensities of 529.9 eV, 531.3 eV and 532.8 eV, respectively [28]. In CuO/BP composite, each characteristic peak had some shift owing to the varied and complicated chemical environment of O. The corresponding deficient oxygen ratios were calculated to be 37.3% and 41.1% respectively for CuO and CuO/BP samples, suggesting that more surface oxygen vacancies were formed on the surface of CuO samples [29]. The concentration of oxygen vacancies is directly corelated with the reduction process from Cu(II) to Cu(I), and when the concentration of Cu(II) decreases, the concentration of oxygen vacancies may increase [30]. Moreover, the reduction process from Cu(II) to Cu(I) is lubricated by the rapid diffusing channel provided by BP [31], demonstrating that introduction of BP enhanced the amount of deficient oxygen. Finally, Fig. 2**F** shows the P 2p spectra of CuO/BP nanocomposite as well as pure BP sample. The P 2p spectrum of pure BP sample exhibited the P $2p_{3/2}$ and P $2p_{1/2}$ doublets at 128.9 and 130.1 eV, respectively, which were the characteristics of the P-P bond within BP. Interestingly, the typical peaks of P 2p exhibited a obvious shift to higher binding energies in the CuO/BP heterostructure. In XPS analysis, the increasing binding energy indicates a lessened screening effect owing to the decrease of electron density [32]. The reduction of electron density surrounding BP was approximately assigned to the electron transfer from BP to CuO through the contact interface. Besides, the peak at 133.6 eV came from the P-O bonding and its intensity increased a lot in the CuO/BP composite, which enabled the few-layer BP matrix to bind strongly with CuO and enhanced the electrochemical performance, especially the sensitivity and stability [33].

2.2. Electrochemical behavior investigation

CuO has been deeply exploited in electrochemical sensing field and performs prominent efficiency in non-enzymatic biosensor [34]. Hence, CuO was deemed as dominant sensing part in the CuO/BP hybrid and the optimal amount of CuO NPs was first investigated using cyclic voltammetry (CV) tests in CS/CuO/GCE for better compounding. As shown in Fig. 3**A**, among four serial concentrations (1.25–5 mg mL^{-1}), CuO NPs at a concentration of 2.5 mg mL^{-1} showed superior detection performance. In accordance, the CuO/BP composites were prepared using 2.5 mg mL^{-1} of CuO NPs solution with different amount of BP. Then, CS/CuO/GCE, CS/BP/GCE and CS/CuO/BP/GCE were used as working electrodes for CV tests to assess the electrocatalytic activity of the heterostructure. As shown in Fig. S4A-**D**, the obvious oxidative and reductive peaks were observed in CuO-based electrodes in contrast with those of CS/BP/GCE. In addition, the corresponding anodic current of CS/CuO/BP/GCE was much higher than that of CS/CuO/GCE even without H_2O_2. As revealed by the XPS spectra of Cu $2p_{3/2}$ (Fig. S3), the fabricated CuO-based electrodes were both consist of Cu(I) and Cu(II) species. The area ratio of [Cu(I)/Cu(I)+Cu(II)] in Cu $2p_{3/2}$ spectrum of CuO/BP sample was as high as 40.5%, which was remarkably higher than pure CuO sample. According to the previous study, the anodic current of CuO-based electrodes whose surface were enriched in Cu(I) can be elaborated as [35,36]:

$$Cu_2O + 2OH^- - 2e^- \rightarrow 2CuO + H_2O \quad (1)$$

After introduction of H_2O_2, the Cu(II) was chemically reduced to Cu (I) as demonstrated through the following the equation:

$$2CuO + H_2O_2 \rightarrow Cu_2O + H_2O + O_2 \quad (2)$$

In such process, the oxidation of Cu(I) occurred as quickly as the reduction of Cu(II) promoted by H_2O_2. As illustrated in Fig. 3**B**, the CS/CuO/BP/GCE had a considerable increase of redox current compared to the other electrodes in 0.1 M NaOH containing 2 mM H_2O_2. In Fig. S4E, with concentration of H_2O_2 increasing, the oxidative current enhanced as well. Since the above reaction between CuO and H_2O_2 was rapid, the CuO/BP hybrid may act as a good intermediate to assist the electron delivery between H_2O_2 and the electrode, facilitating the enhancement of the anodic peak current.

The improvement of electrochemical performance was most probably attributed to unique heterostructure of CuO/BP. Three factors can be assigned for superior electrochemical behavior of CS/CuO/BP/GCE. Foremost, as discussed above, Cu(I)/Cu(II) redox pair play a vital role in the electrochemical response in H_2O_2 detecting. Importantly, the Cu(I) species on the electrode surface increased after integrating BP with CuO as shown in the XPS result. Therefore, plenty amounts of Cu(I)/Cu(II) lubricated the electrochemical detection process magnificently. Moreover, the significantly increased amount of deficient oxygen on the surface of CuO/BP nanocomposite, as proven in the deficient oxygen ratio in the XPS spectra of O 1 s, contributed a lot to facilitate the electrochemical sensing performance owing to improving redox capability. This can be elucidated by the fact that increased deficient oxygen ratio enhances oxygen vacancies, which work as electron mediator in transferring electrons [37]. Referring to morphological aspect, the wrinkled structure of BP NSs was applied to provide a wide, open, and continuous place, which promoted anchoring sites for sensitive materials to fully contact with target analytes. Finally, abundant amounts of heterojunctions were formed at the interface of CuO and BP which built the rapid diffusing channel for the transfer of electron between CuO NPs and H_2O_2, in this way, extraordinary recognizing capacity and ultralow detection limit can be achieved.

To continue, the concentration ratio of CuO and BP was explored to optimize the monitoring performance. In Fig. 3**C**, CuO4-BP1 electrode represented the highest value of reduction peak current. The result confirmed that higher proportion of CuO in the modified electrodes

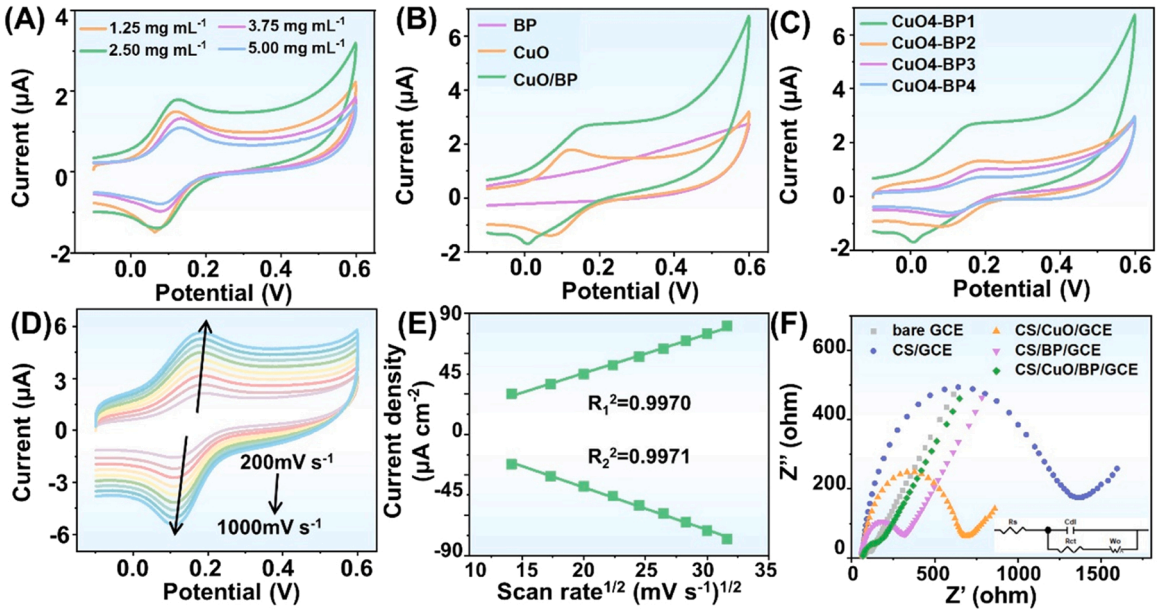

Fig. 3. Electrochemical properties of the modified electrodes: (A) CVs of pure CS/CuO/GCE with different concentrations of CuO NPs; (B) CVs of CS/CuO/GCE, CS/BP/GCE and CS/CuO/BP/GCE, respectively; (C) CVs of CS/CuO/BP/GCE with different CuO/BP ratios; (D) CVs of CS/CuO/BP/GCE at various scan rates; (E) oxidation or reduction peak current density vs. the square root of scan rates. All CVs were tested in 0.1 M NaOH with 2 mM H_2O_2. (F) EIS of bare GCE, CS/GCE, CS/CuO/GCE, CS/BP/GCE and CS/CuO/BP/GCE in 5 mM $[Fe(CN)_6]^{-3/-4}$ (1:1) + 0.1 M KCl.

enhanced the catalytic activity and the catalytic role of CuO was extremely significant in the reaction process of H_2O_2 oxidation. Furthermore, BP played an auxiliary role who provided both effective electronic channels and amounts of active sites, facilitating the electrochemical sensing for H_2O_2 determination. While, too many BP NSs may consequently block the pathway for sensing material contacting with the target molecules. Therefore, the optimized CuO4-BP1 electrode was selected for further electrochemical studies toward H_2O_2 determination.

Subsequently, the CVs of the as-prepared CS/CuO/BP/GCE at various scan rates (200–1000 mV s^{-1}) were investigated in 2 mM H_2O_2 solution (Fig. 3**D**). The corresponding density of the redox peak linearly increased along with the square root of scan rate (Fig. 3**E**), and the correlation coefficients (R^2) were determined to be 0.9970 and 0.9971 for oxidation and reduction peaks, respectively, illustrating a diffusion-controlled electrochemical process [38]. Controlled by such process,the transfer of the generated electrons improved a lot. Afterwards,the electron transport ability of different electrodes was explored and compared via the EIS technique. Fig. 3**F** displayed the Nyquist plots of CS/CuO/BP/GCE compared with CS/CuO/GCE, CS/BP/GCE, CS/GCE and bare GCE in the presence of redox probe $[Fe(CN)_6]^{3-/4-}$. The capability of electron transfer on the different electrodes can be presented by the semicircle of EIS, which signifies the resistance originating from charge transfer limitation (R_{ct}). Here, a simple equivalent circuit was applied to model the impedance data in the presence of redox couples and also to calculate the exact R_{ct} value of each curve, which was shown in the inset of Fig. 3F. In this circuit, R_s, C_{dl}, and R_{ct} signified the solution resistance, the double layer capacitance, and the charge transfer resistance, respectively. The results demonstrated that the bare GCE attained an electron-transfer resistance of about 44.79 Ω, indicating a very low electron-transfer resistance to the redox probe dissolved in the electrolyte. When modified with CS, the semicircle increased to 1161 Ω compared to the bare GCE, implying bad electrical conductivity of CS. The resistance of CS/CuO/BP/GCE was 100.7 Ω, much lower than the resistance of CS/CuO/GCE and CS/BP/GCE (555.1 and 238.4 Ω, respectively), which may be attributed to the CuO/BP heterostructure with larger electrode contact area and accelerated charge transfer.

To determine the response efficiency and sensitivity of the as-prepared electrode for H_2O_2 detection, amperometric measurements were further evaluated. Owing to the fact that the applied potential in chronoamperometry has a significant influence on the sensitivity of an electrochemical sensor [39], the current-time (i–t) test was first conducted at different applied potentials in CS/CuO/BP/GCE, since the current of CV curve reached to a platform at 0.1–0.3 V (green line in Fig. 3C), indicating supreme conducting and sensing ability. Fig. 4**A&4B** displayed the amperometric response and corresponding calibration curves of CS/CuO/BP/GCE upon successive addition of H_2O_2 with increasing concentrations into 0.1 M NaOH solution at different potentials in range of 0.1–0.3 V. As compared, the current-time (i–t) curve under 0.3 V showed the highest current response due to more transferring electron provided by higher potential, approximately [40]. Accordingly, all the current responses were monitored under 0.3 V for a better performance.

To obtain a clear comparison of the advantage of the CuO/BP composite, CS/CuO/GCE, CS/BP/GCE and CS/CuO/BP/GCE were further served as working electrodes for chronoamperometry tests in 0.1 M NaOH solution. The i–t and corresponding calibration curves were plotted in Fig. 4**C&4D** and Fig. S5 displayed the calibration curves at lower concentration in detail, indicating superior detection capacity of the heterostructure for CuO/BP, which was consistent with the result in CVs. On the basis of the above calibration curves as exhibited in Fig. 4**B&D**, the sensitivity, linear range, correlation coefficients (R^2), and the theoretical limit of detection (LOD) of the different electrodes in this work were summarized in Table 1.

Referring to potential, the sensitivity increased as the voltage elevated from 0.1 V to 0.3 V, meanwhile, the detecting limit became lower, which may be attributed to enhanced electron mobility for higher potential [40]. At applied voltage of 0.3 V, the CS/CuO/BP/GCE exhibited excellent sensitivity of 138.00 (0.2–99.8 μM) and 11.32 (99.8–9339.8 μM) μA mM^{-1} cm^{-2}, as well as a low theoretical detection limit of 0.112 μM. Compared with CS/CuO/GCE and CS/BP/GCE, the superiority of CS/CuO/BP/GCE was largely assigned to sufficient synergistic effect between CuO and BP, which contributed to enhanced surface adsorption and efficient electron transfer for better sensing performance. Moreover, the actual detection limit was estimated to be

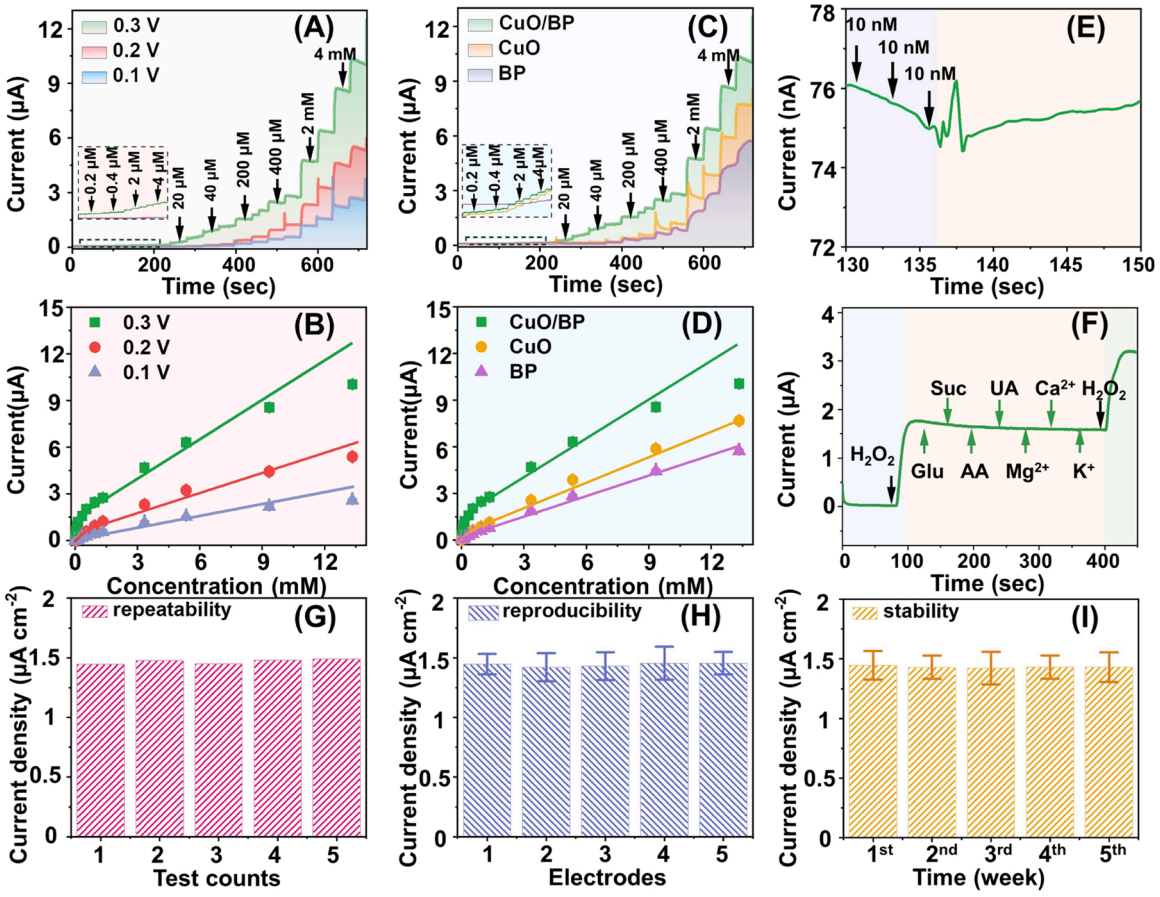

Fig. 4. Electrocatalytic performance of the supposed electrodes: (A) i–t curves with successive additions of H_2O_2 at an applied potential of 0.3 V, 0.2 V, 0.1 V for CS/CuO/BP/GCE; (B) Calibration curves for i–t curves of (A); (C) i–t curves with successive additions of H_2O_2 for CS/CuO/BP/GCE, CS/CuO/GCE, CS/BP/GCE; (D) Calibration curves for i–t curves of (C); (E) LOD study with additions of H_2O_2 for CS/CuO/BP/GCE at an applied potential of 0.3 V; (F) Selectivity study for CS/CuO/BP/GCE in the presence of 0.5 mM H_2O_2 and 1 mM interfering chemicals; (G) Repeatability for single CS/CuO/BP/GCE; (H) Reproducibility for five CS/CuO/BP/GCEs; and (I) Long-term stability for CS/CuO/BP/GCEs every week, all curves were tested in 0.1 M NaOH.

30 nM (Fig. 4**E**), indicating the supreme sensitivity of the CS/CuO/BP/GCE (signal-to-noise ratio (S/N) = 3). Meanwhile, the sensing performance of the prepared CS/CuO/BP/GCE are also compared with some typical non-enzymatic H_2O_2 biosensors. Compared with various electrochemical biosensors in previous literatures (Table S1), the ultrawide linear range and extremely low detection limit of CS/CuO/BP/GCE indicated the electrocatalytic ability of such heterostructure with abundant active sites and effective electronic channels. Furthermore, this absolutely confirmed its promising potential for application in real-time detection of H_2O_2, particularly in inflammatory diseases with pathological H_2O_2 elevation.

In addition, the selectivity of the as-prepared sensor was examined in Fig. 4**F** by adding 20-fold concentration of potentially interfering biomolecules in the electrolyte such as glucose (Glu), sucrose (Suc), uric acid (UA), ascorbic acid (AA), Ca^{2+}, Mg^{2+}, and K^+ during the amperometry test. The sensor detected a negligible interference compared with two injections 0.5 mM of H_2O_2 in the solution, demonstrating the good selectivity of the CS/CuO/BP/GCE. Subsequently, the repeatability was evaluated by measuring a single CS/CuO/BP/GCE for five times to detect 20 μM of H_2O_2 in 0.1 M NaOH solution, which exhibited a relative standard deviation (RSD) of 3.3% (Fig. 4**G**). Besides, reproducibility was investigated by examining five electrodes in the same condition. The RSD was determined to be 1.1% (Fig. 4**H**). Ultimately, the long-term stability of the supposed electrode was illustrated in Fig. 4**I** by continuously measuring the response to 20 μM H_2O_2 in 0.1 M NaOH solution for 5 weeks. The CS/CuO/BP/GCE at 5^{th} week could maintain as high response value as > 98% level compared to that at 1^{st} week. All these results suggested that such electrochemical biosensor exhibited a favorable sensing performance in detection of H_2O_2, demonstrating the excellent practicability of the proposed H_2O_2 biosensor.

2.3. Feasibility study of the electrochemical biosensor

With respect to the practicability and feasibility of the electrochemical biosensor for early diagnosis for periodontitis, all sensing activity ought to implement under supposed pathological environment. Before all practical tests, the CS/CuO/BP/GCE was examined in 0.01 M PBS (pH = 8.5), which simulated the salivary alkaline environments for patients with periodontitis [41]. As shown in Fig. S6, the CV curve confirmed the outstanding electrochemical catalytic effect of such hybrid under alkalescent physiological environment, comparing with the bare CS/CuO/GCE. Moreover, the selectivity in alkaline PBS was displayed in Fig. S7, further proving its extraordinary performance as an electrochemical biosensor. It was worth mentioning that though the current reached a platform stage at 0.25 V in the CV curve (Fig. S6), the selectivity test attained inferior performance at the same potential. This may be assigned to the fact that lower potential lacked distinct recognizing capability in PBS solution. As a result, wide range of potentials (0.15–0.65 V) were investigated and supreme selective competence was obtained under 0.55 V (Fig. S7). Subsequently, Fig. S8 presented the i-t and corresponding calibration curves of the supposed electrode (CS/CuO/BP/GCE, 0.55 V) with the excellent sensitivity of 1.70 (40–480 μM) and 0.58 (480–9280 μM) μA mM^{-1} cm^{-2}, as well as a low theoretical detection limit of 3.48 μM. which indicated its brilliant

Table 1
The summary of sensing performance among different electrodes for detecting H_2O_2 in NaOH solution in this work.

Working electrode	Applied potential (V)	Theoretical LOD (μM)	Detection range (μM)	Sensitivity (μA mM^{-1} cm^{-2})	R^2
CS/CuO/BP/GCE (in NaOH)	0.10	1.70	2–338	8.56	0.9989
			338–5338	5.15	0.9953
CS/CuO/BP/GCE (in NaOH)	0.20	1.14	2–538	17.41	0.9853
			538–5338	8.11	0.9926
CS/CuO/BP/GCE (in NaOH)	0.30	0.112	0.2–99.8	138.00	0.9908
			99.8–9339.8	11.32	0.9830
CS/CuO/GCE (in NaOH)	0.30	0.152	0.2–19.8	63.98	0.9898
			19.8–13339.8	8.88	0.9952
CS/BP/GCE (in NaOH)	0.30	0. 83	2–18	13.63	0.9797
			18–5338	7.54	0.9990
CS/CuO/BP/GCE (in PBS)	0.55	3.48	40–480	1.70	0.9964
			480–9280	0.58	0.9943

sensing performance in the mimicking environment of periodontitis.

As presented in Fig. 5**A**, the clinical practicability for early diagnosis of periodontitis was investigated at a biofluid level and cellular level. The artificial saliva was first applied as a simulated body fluid for H_2O_2 biosensing with CS/CuO/BP/GCE, since it mimics the exact environment of saliva which contains numerous ions such as Na^+, K^+, Ca^{2+}, NH_4^+ and Cl^-. Consequently, this test evaluated detection performance of the supposed biosensor in more complicated surroundings. The recovery was assessed by mixing artificial saliva with three different concentrations of H_2O_2. The results listed in Table S2 confirmed the recoveries of 98.1–99.5% for artificial saliva, suggesting its great potential for H_2O_2 determination for biological application.

In order to further explore the CS/CuO/BP/GCE for practical applications, the sensor was applied to monitor H_2O_2 in human saliva and GCF of 10 patients (from Department of Periodontology, Hospital of Stomatology, Jilin University). Samples from ten healthy people were also detected as control. The protocol for sample collection was approved by the Institutional Review Board of Jilin University, Hospital of Stomatology. Informed consents were provided by all individuals involved in this study prior to the sample collection. Each clinical sample was measured by three different CS/CuO/BP/GCEs. As shown in Fig. 5**B**, after a 10 μL aliquot of clinic GCF sample was added into 10 mL of 0.01 M PBS solution. the response current of healthy people was very close and low (at approximately 0.01 nA). In contrast, the corresponding current intensity of samples from patients with periodontitis rendered a significantly higher (> 1.5 nA) current intensity. The investigation of saliva samples demonstrated the similar condition as GCF samples except lower current response for pathological samples (Fig. 5**C**). The current intensity difference of patients may attribute to the closer position of gingival crevicular to the teeth, which enables the easier collection and enrichment of biofluid. Hence, this sensor could be used not only to monitor H_2O_2 in oral fluid such as GCF and saliva, but also to distinguish between healthy people and periodontitis patients with optimal threshold for accurate diagnosis of periodontitis.

With respect to the microcosmic level, H_2O_2 is a biomarker for inflammatory cells since it is closely associated with dysfunction of cellular metabolism by NADPH oxidase enzymes [42] In periodontitis, such enzyme exists in many cell types, especially in immune cells or fibroblasts. Therefore, macrophages (murine Raw 264.7 cell line) and fibroblasts (human gingival fibroblast cells, HGF cells) were utilized as cell models for H_2O_2 detection by CS/CuO/BP/GCE via the amperometric technique. To guarantee the adaptability of this biosensor in the cellular level, different stimulants including LPS, AA and PMA were used to stimulate two kinds of cells to produce H_2O_2, as they can disrupt intracellular redox homeostasis of cells. Fig. 5**D** showed the current response of CS/CuO/BP/GCE in presence of cells in 0.01 M PBS. With the addition of LPS, the current response increased, indicating release of H_2O_2 from the cells (curve a&b). However, with the introduction of both stimulants and catalase (a selective scavenger of H_2O_2), no current increase could be spotted (curve c&d), further proving that the current increase was owing to H_2O_2 released from the cells. Moreover, the current response of Raw 264.7 was stronger than that of HGF cells, owing to lower cells amount (half dish of cells were implemented independently with approximately 3.5×10^6 Raw 264.7 cells or 1×10^6 HGF cells). The same situation was spotted when AA and PMA were applied as stimulants (Fig. 5**E&F**). Interestingly, PMA contributed to weaker current response compared with LPS and AA, which was in accordance with previous literature [43]. These results demonstrated that stimulants can induce living Raw 264.7 or HGF cells to generate H_2O_2, which can be scavenged by catalase. The corresponding process for Fig. 5**D-F** was visualized by H_2O_2 fluorescence probe DCFH-DA in living cells. As shown in Fig. 5**G**, the Raw 264.7 or HGF cells displayed weaker intensity of fluorescence without stimulating agent. However, when the cells were stimulated by AA, LPS or PMA, intense green fluorescence was observed. Interestingly, groups with integration of stimulants and catalase showed similar fluorescence signal as groups without any stimulation. The confocal microscopy investigation enhanced the reliability for feasibility of biosensor at the in *vitro* cellular level. Overall, the designed biosensor could be applied to monitor H_2O_2 and possessed extraordinary potential in inflammatory conditions.

So far, numerous efforts had been done for periodontitis diagnosis based on biomarkers such as proteins [44–46], enzymes [26,47], ions [48,49], genes [50,51], endotoxins [52], *etc*. This work also presented smart strategy to detect H_2O_2 for early recognition of periodontitis, which provided favorable convenience, sensitivity and feasibility. However, point-of-care testing (POCT) platform would still be the primary trend in the near future [53], which emphasizes flexibility and portability of certain biosensors. Therefore, further studies should focus on wearable and integrative devices for diagnosis and treatment of diseases much more than periodontitis.

3. Conclusion

To sum up, this work modifies classical GCE with combination of heterostructure of CuO NPs and BP NSs to detect H_2O_2 for timely diagnosis of early periodontitis. Using the 2D BP NSs as supporting materials to load CuO NPs, the fabricated CS/CuO/BP/GCE exhibits the best electrocatalytic activity toward H_2O_2 oxidation on account of the unique surface configuration presenting synergistic effects that enhanced H_2O_2 adsorption and interfacial electron transfer. This non-enzymatic electrochemical sensor holds favorable selectivity, extremely wide concentration range and low practical LOD of 30 nM for monitoring H_2O_2. Moreover, this sensor can also be utilized for real-time detection of H_2O_2 secreted from macrophages and gingival fibroblasts upon stimulation. More importantly, this work provides an interesting and optimal method for recognizing the early periodontitis from oral biofluids such as saliva and GCF, which are quite accessible in clinic to realize a non-invasive diagnosis. Therefore, this work offers brilliant scheme to apply efficient biosensor in diagnosis and treatment of diseases. Overall, the CuO/BP modified sensor for H_2O_2 detection could not only be used for the early diagnosis of periodontitis, but also be extended for other inflammatory diseases.

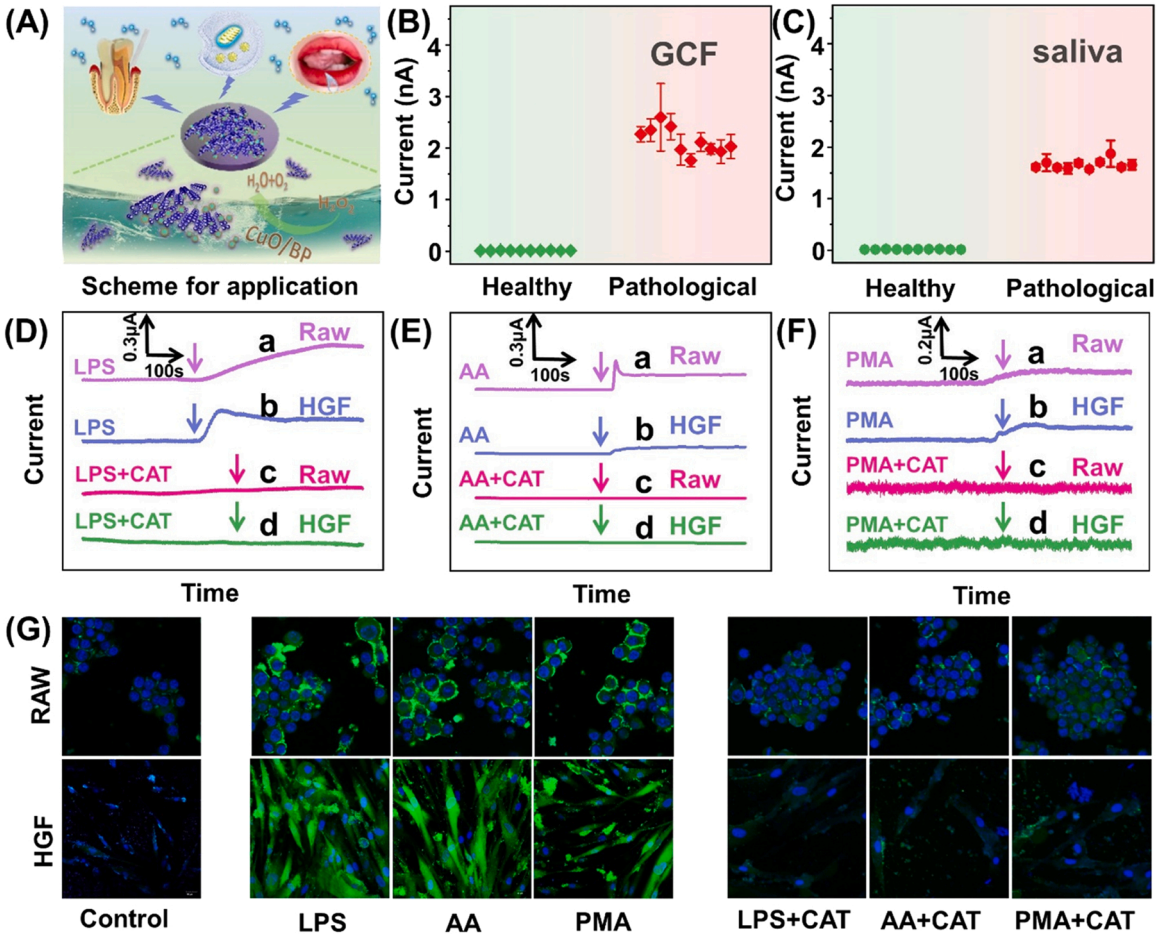

Fig. 5. (A) Scheme of the biofluid and cell study for the CS/CuO/BP/GCE. (B-C) Responses of three different electrodes to (B) human saliva and (C) GCF samples taken from 10 patients and 10 healthy people. (D-F) Amperometric response of H_2O_2 released from cells stimulated by (D) AA, (E) LPS or (F) PMA in 0.01 M PBS without and with 300 U mL^{-1} catalase. (G) DYPI and DCFH-DA confocal microscopy images of Raw 264.7 and HGF cells stimulated by AA, LPS or PMA without and with catalase.

CRediT authorship contribution statement

Kun Wang: Data curation, Writing – original draft. **Yue Sun**: Validation, Writing – original draft. **Yu Qi**: Investigation, Data curation. **Yuhong Zhang**: Software, Formal analysis. **Qingqing Zhou**: Resources, Formal analysis. **Wei Zhang**: Visualization. **Fanrou Zhang**: Visualization, Supervision. **Wenzhou Xu**: Supervision. **Biao Dong**: Validation. **Chunyan Li**: Supervision. **Lin Wang**: Conceptualization, Writing – review & editing, Funding acquisition. **Lin Xu**: Conceptualization, Writing – review & editing, Project administration.

Declaration of Competing Interest

The authors declare that they have no known competing financial interests or personal relationships that could have appeared to influence the work reported in this paper.

Acknowledgments

This work was supported by National Science Foundation of China (82170998, 61874049 and 61775080), China Postdoctoral Science Foundation 2017T100213, General Program of Natural Science Foundation of Jilin Province (20200201356JC, 20200201317JC, 20180101210JC and 20200801017GH), seed grant from Jilin University School of Dentistry, and the Fundamental Research Funds for the Central Universities.

Appendix A. Supporting information

Supplementary data associated with this article can be found in the online version at doi:10.1016/j.snb.2021.131298.

References

[1] J. Kim, S. Amar, Periodontal disease and systemic conditions: a bidirectional relationship, Odontology 94 (2006) 10–21.
[2] W. He, M. You, W. Wan, F. Xu, F. Li, A. Li, Point-of-care periodontitis testing: biomarkers, current technologies, and perspectives, Trends Biotechnol. 36 (2018) 1127–1144.
[3] W. Pan, Q. Wang, Q. Chen, The cytokine network involved in the host immune response to periodontitis, Int. J. Oral Sci. 11 (2019) 1–13.
[4] C. Liu, L. Mo, Y. Niu, X. Li, X. Zhou, X. Xu, The role of reactive oxygen species and autophagy in periodontitis and their potential linkage, Front. Physiol. 8 (2017) 439.
[5] R.J. Waddington, R. Moseley, G. Embery, Periodontal disease mechanisms: reactive oxygen species: a potential role in the pathogenesis of periodontal diseases, Oral Dis. 6 (2000) 138–151.
[6] J. Meier, E.M. Hofferber, J.A. Stapleton, N.M. Iverson, Hydrogen peroxide sensors for biomedical applications, Chemosensors 7 (2019) 64.
[7] W. Wang, H. Tang, Y. Wu, Y. Zhang, Z. Li, Highly electrocatalytic biosensor based on Hemin@ AuNPs/reduced graphene oxide/chitosan nanohybrids for non-enzymatic ultrasensitive detection of hydrogen peroxide in living cells, Biosens. Bioelectron. 132 (2019) 217–223.
[8] X. Zhang, C.J. Zhang, A. Abas, Y. Zhang, X. Mu, J. Zhou, Q. Su, W. Lan, E. Xie, Ag nanoparticles enhanced vertically-aligned CuO nanowire arrays grown on Cu foam for stable hybrid supercapacitors with high energy density, Electrochim. Acta 296 (2019) 535–544.
[9] H. Duan, D. Xu, W. Li, H. Xu, Study of the redox properties of noble metal/Co 3 O 4 by electrical conductivity measurements, Catal. Lett. 124 (2008) 318–323.

[10] Y. Song, B. Xu, T. Liao, J. Guo, Y. Wu, Z. Sun, Electronic structure tuning of 2D metal (hydr) oxides nanosheets for electrocatalysis, Small 17 (2021) 2002240.
[11] S. Mallakpour, M. Madani, A review of current coupling agents for modification of metal oxide nanoparticles, Prog. Org. Coat. 86 (2015) 194–207.
[12] S. Li, L. Xie, M. He, X. Hu, G. Luo, C. Chen, Z. Zhu, Metal-organic frameworks-derived bamboo-like CuO/In2O3 heterostructure for high-performance H2S gas sensor with low operating temperature, Sens. Actuators B Chem. 310 (2020), 127828.
[13] J.S. Kumar, S. Ghosh, N.C. Murmu, N. Mandal, T. Kuila, Electrochemical detection of H2O2 using copper oxide-reduced graphene oxide heterostructure, J. Nanosci. Nanotechnol. 19 (2019) 5295–5302.
[14] K.S. Novoselov, A.K. Geim, S.V. Morozov, D. Jiang, Y. Zhang, S.V. Dubonos, I. V. Grigorieva, A.A. Firsov, Electric field effect in atomically thin carbon films, Science 306 (2004) 666–669.
[15] A. Bolotsky, D. Butler, C. Dong, K. Gerace, N.R. Glavin, C. Muratore, J.A. Robinson, A. Ebrahimi, Two-dimensional materials in biosensing and healthcare: from in vitro diagnostics to optogenetics and beyond, ACS Nano 13 (2019) 9781–9810.
[16] Y. Zhang, Y. Zheng, K. Rui, H.H. Hng, K. Hippalgaonkar, J. Xu, W. Sun, J. Zhu, Q. Yan, W. Huang, 2D black phosphorus for energy storage and thermoelectric applications, Small 13 (2017) 1700661.
[17] S. Yan, B. Wang, Z. Wang, D. Hu, X. Xu, J. Wang, Y. Shi, Supercritical carbon dioxide-assisted rapid synthesis of few-layer black phosphorus for hydrogen peroxide sensing, Biosens. Bioelectron. 80 (2016) 34–38.
[18] Y. Zhao, Y.-H. Zhang, Z. Zhuge, Y.-H. Tang, J.-W. Tao, Y. Chen, Synthesis of a poly-L-lysine/black phosphorus hybrid for biosensors, Anal. Chem. 90 (2018) 3149–3155.
[19] Y. Zhao, Z. Zhuge, Y.-H. Tang, J.-W. Tao, Synthesis of a CuNP/chitosan/black phosphorus nanocomposite for non-enzymatic hydrogen peroxide sensing, Analyst 145 (2020) 7260–7266.
[20] M. Vanni, M. Caporali, M. Serrano-Ruiz, M. Peruzzini, Catalysis mediated by 2D black phosphorus either pristine or decorated with transition metals species, Surfaces 3 (2020) 132–167.
[21] R. He, J. Hua, A. Zhang, C. Wang, J. Peng, W. Chen, J. Zeng, Molybdenum disulfide–black phosphorus hybrid nanosheets as a superior catalyst for electrochemical hydrogen evolution, Nano Lett. 17 (2017) 4311–4316.
[22] A. Nezamzadeh-Ejhieh, M. Karimi-Shamsabadi, Decolorization of a binary azo dyes mixture using CuO incorporated nanozeolite-X as a heterogeneous catalyst and solar irradiation, Chem. Eng. J. 228 (2013) 631–641.
[23] S. Wang, H. Xu, L. Qian, X. Jia, J. Wang, Y. Liu, W. Tang, CTAB-assisted synthesis and photocatalytic property of CuO hollow microspheres, J. Solid State Chem. 182 (2009) 1088–1093.
[24] S. Reddy, B.E.K. Swamy, H. Jayadevappa, CuO nanoparticle sensor for the electrochemical determination of dopamine, Electrochim. Acta 61 (2012) 78–86.
[25] J. Ghijsen, L.-H. Tjeng, J. van Elp, H. Eskes, J. Westerink, G.A. Sawatzky, M. T. Czyzyk, Electronic structure of Cu 2 O and CuO, Phys. Rev. B 38 (1988) 11322.
[26] S. Park, K. Park, H.S. Na, J. Chung, H. Yang, Washing-and separation-free electrochemical detection of Porphyromonas gingivalis in saliva for initial diagnosis of periodontitis, Anal. Chem. 93 (2021) 5644–5650.
[27] X. Wang, Q. Li, P. Shi, J. Fan, Y. Min, Q. Xu, Nickel nitride particles supported on 2D activated graphene–black phosphorus heterostructure: an efficient electrocatalyst for the oxygen evolution reaction, Small 15 (2019) 1901530.
[28] X. Zhou, L. Xu, J. Lv, S. Yang, S. Zhu, X. Chen, X. Sun, B. Dong, X. Bai, G. Lu, Au anchored three-dimensional macroporous NiO@ CuO inverse opals for in-situ sensing of hydrogen peroxide secretion from living cells, Sens. Actuators B Chem. 297 (2019), 126729.
[29] R. Xing, Q. Li, L. Xia, J. Song, L. Xu, J. Zhang, Y. Xie, H. Song, Au-modified three-dimensional In 2 O 3 inverse opals: synthesis and improved performance for acetone sensing toward diagnosis of diabetes, Nanoscale 7 (2015) 13051–13060.
[30] Y. Maimaiti, M. Nolan, S.D. Elliott, Reduction mechanisms of the CuO (111) surface through surface oxygen vacancy formation and hydrogen adsorption, Phys. Chem. Chem. Phys. 16 (2014) 3036–3046.
[31] Q. Bi, K. Hu, J. Chen, Y. Zhang, M.S. Riaz, J. Xu, Y. Han, F. Huang, Black phosphorus coupled black titania nanocomposites with enhanced sunlight absorption properties for efficient photocatalytic CO_2 reduction, Appl. Catal. B Environ. 295 (2021), 120211.
[32] M. Zhu, S. Kim, L. Mao, M. Fujitsuka, J. Zhang, X. Wang, T. Majima, Metal-free photocatalyst for H2 evolution in visible to near-infrared region: black phosphorus/graphitic carbon nitride, J. Am. Chem. Soc. 139 (2017) 13234–13242.
[33] J. Li, L. Wang, X. He, J. Wang, Effect of pore size distribution of carbon matrix on the performance of phosphorus@ carbon material as anode for lithium-ion batteries, ACS Sustain. Chem. Eng. 4 (2016) 4217–4223.
[34] K. Atacan, M. Özacar, Construction of a non-enzymatic electrochemical sensor based on CuO/g-C3N4 composite for selective detection of hydrogen peroxide, Mater. Chem. Phys. 266 (2021), 124527.
[35] W.-Z. Le, Y.-Q. Liu, Preparation of nano-copper oxide modified glassy carbon electrode by a novel film plating/potential cycling method and its characterization, Sens. Actuators B Chem. 141 (2009) 147–153.
[36] P.S. Adarakatti, V. Udayakumar, Engineering of CuO/ZrO2 nanocomposite-based electrochemical sensor for the selective detection of hydrogen peroxide, Ionics (2021) 1–14.
[37] W. Zhao, W. Wang, H. Shi, 2D/2D Z-scheme BiO1-XBr/g-C3N4 heterojunction with rich oxygen vacancies as electron mediator for enhanced visible-light degradation activity, Appl. Surf. Sci. 528 (2020), 146925.
[38] W.H. Antink, Y. Choi, K. Seong, Y. Piao, Simple synthesis of CuO/Ag nanocomposite electrode using precursor ink for non-enzymatic electrochemical hydrogen peroxide sensing, Sens. Actuators B Chem. 255 (2018) 1995–2001.
[39] Q. Wang, Y. Yang, F. Gao, J. Ni, Y. Zhang, Z. Lin, Graphene oxide directed one-step synthesis of flowerlike graphene@ HKUST-1 for enzyme-free detection of hydrogen peroxide in biological samples, ACS Appl. Mater. Interfaces 8 (2016) 32477–32487.
[40] Y.J. Yang, W. Li, X. Chen, Highly enhanced electrocatalytic oxidation of glucose on Cu (OH) 2/CuO nanotube arrays modified copper electrode, J. Solid State Electrochem. 16 (2012) 2877–2881.
[41] R.M. Patel, S. Varma, G. SuRaGiMath, S. ZoPe, Estimation and comparison of salivary calcium, phosphorous, alkaline phosphatase and pH levels in periodontal health and disease: a cross-sectional biochemical study, J. Clin. Diagn. Res. JCDR 10 (2016) ZC58.
[42] M.F. Ross, G.F. Kelso, F.H. Blaikie, A.M. James, H.M. Cocheme, A. Filipovska, T. Da Ros, T.R. Hurd, R.A.J. Smith, M.P. Murphy, Lipophilic triphenylphosphonium cations as tools in mitochondrial bioenergetics and free radical biology, Biochem 70 (2005) 222–230.
[43] M. Li, H. Gao, X. Wang, Y. Wang, H. Qi, C. Zhang, A fluorine-doped tin oxide electrode modified with gold nanoparticles for electrochemiluminescent determination of hydrogen peroxide released by living cells, Microchim. Acta 184 (2017) 603–610.
[44] W. He, M. You, Z. Li, L. Cao, F. Xu, F. Li, A. Li, Upconversion nanoparticles-based lateral flow immunoassay for point-of-care diagnosis of periodontitis, Sens. Actuators B Chem. 334 (2021), 129673.
[45] D. Liu, L. Zhou, L. Huang, Z. Zuo, V. Ho, Y. Lu, X. Chen, J. Zhao, D. Qian, H. Liu, Microfluidic integrated capacitive biosensor for C-Reactive Protein label-free and real-time detection, Analyst (2021).
[46] H. Lähteenmäki, K.A. Umeizudike, A.M. Heikkinen, I.T. Räisänen, N. Rathnayake, G. Johannsen, T. Tervahartiala, S.O. Nwhator, T. Sorsa, aMMP-8 point-of-care/chairside oral fluid technology as a rapid, non-invasive tool for periodontitis and peri-implantitis screening in a medical care setting, Diagnostics 10 (2020) 562.
[47] A. Svärd, J. Neilands, E. Palm, G. Svensäter, T. Bengtsson, D. Aili, Protein-functionalized gold nanoparticles as refractometric nanoplasmonic sensors for the detection of proteolytic activity of Porphyromonas gingivalis, ACS Appl. Nano Mater 3 (2020) 9822–9830.
[48] E.E. Totu, I. Isildak, A.C. Nechifor, C.M. Cristache, M. Enachescu, New sensor based on membranes with magnetic nano-inclusions for early diagnosis in periodontal disease, Biosens. Bioelectron. 102 (2018) 336–344.
[49] C. Zhao, R. Shi, J. Wu, X. Luo, X. Liu, Point-of-care detection of salivary nitrite based on the surface plasmon-assisted catalytic coupling reaction of aromatic amines, Biosensors 11 (2021) 223.
[50] X. Xu, X. Li, Q. Chen, J. Yuan, Detection of Treponema denticola in chronic periodontitis by quantitative real-time polymerase chain reaction, J. Nanosci. Nanotechnol. 20 (2020) 1463–1469.
[51] J. Yuan, Q. Chen, X. Xu, Rapid method for the detection of Porphyromonas gingivalis in chronic periodontitis, Nanosci. Nanotechnol. Lett. 11 (2019) 689–695.
[52] D. Han, S. Xie, A. Steckl, Development of point-of-care lateral flow assay devices for salivary endotoxin detection, in: DECS Meeting Abstract, IOP Publishing, 2021, p. 1392.
[53] C. Dincer, R. Bruch, A. Kling, P.S. Dittrich, G.A. Urban, Multiplexed point-of-care testing–xPOCT, Trends Biotechnol. 35 (2017) 728–742.

Kun Wang received her B.S. degree from Jilin University in 2021. She is currently studying for a Ph.D. degree at Jilin University. Her research interest is electrochemical biosensing for diagnosis of oral diseases.

Yue Sun received her Ph.D. degree from Jilin University in 2020. She is currently working at School of Dentistry, Jilin University. Her research interest is nanomaterials for biomedical application.

Wenzhou Xu received his Ph.D. degree from Jilin University in 2019. He is currently working at Hospital of Stomatology, Jilin University. His research interest is diagnosis and treatment of periodontitis.

Wei Zhang received her B.S. degree from Mudanjiang Medical College in 2020. She is currently studying for a M.S. degree at Jilin University. Her research interest is s electrochemical biosensing for diagnosis of oral diseases.

Fanrou Zhang received her B.S. degree from Jilin University in 2020. She is currently studying for a M.S. degree at Jilin University. Her research interest is electrochemical biosensing for diagnosis of oral diseases.

Yu Qi received his B.S. degree from Jilin University in 2021. He is currently studying for a Ph.D. degree at Jilin University. His research interest is the gas sensor.

Yuhong Zhang received her M.S. degree from Jilin Normal University in 2020. She is currently studying for a Ph.D.degree at Jilin University. Her research interest is the solar cell.

Qingqing Zhou received her B.S. degree from Jilin University in 2017. She is currently studying for a Ph.D. degree at Jilin University. Her research interest is the gas sensor.

Biao Dong received his Ph.D. degree from Changchun Institute of Physics, CAS in 2008. He is currently working as professor, master tutor, and doctoral supervisor at the Jilin University of electronic science and engineering college.

Chunyan Li received her Ph.D. degree from Jilin University in 2009. She is currently working as chief physician at Hospital of Stomatology, Jilin University. Meanwhile, she is hired as the professor for School of Stomatology, Jilin University.

Lin Wang received his Ph.D. degree in Dentistry from Jilin University in 2011. He is the current vice dean in School of Dentistry, Jilin University. In addition, he also serves as professor, master tutor, doctoral supervisor for School of Dentistry, Jilin University. He obtained honor titled as Jilin university youth science and technology association member.

Lin Xu had a doctorate in physics electronics of Jilin University in 2011. She is the current Jilin University professor, master tutor, doctoral supervisor for institute of electronics and deputy director for the department of biomedical engineering. She obtained honor titled as Jilin university youth science and technology association member.